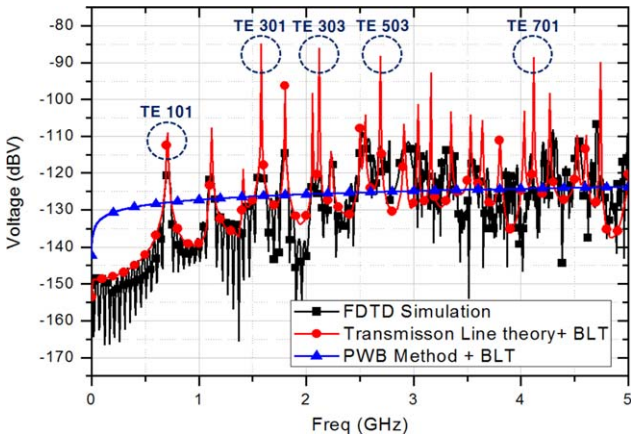

Figure 3 Voltage responses on the loaded TL of PCB according to the analysis methods. [Color figure can be viewed in the online issue, which is available at wileyonlinelibrary.com]

1 mm, respectively, with the loaded resistors of $Z_0 = Z_L = 82.75\ \Omega$.

Figure 3 delineates the voltage response on the loaded resistor of PCB. The analyzed result using the combination of equivalent TL theory and BLT equation is nearly the same as that obtained from the commercially available software. In addition, it can be expected that the result obtained from the analysis using the combination of PWB method and BLT equation is approximately approaching the average values of the other data. Especially in high frequency region of Figure 3, it is seen that the accuracy of PWB method and BLT equation becomes higher. By comparing the resonant frequencies of Figures 3 and 4 it is guaranteed that the PCB structure given in this article does not affect the original resonant frequency when the interior of shielding enclosure is empty. Hence, the two methods mentioned in Sections 2.1 and 2.2 lead to the reliability of the SE analysis inside shielding cavities.

In addition, we have saved a required time consumption and computer resources caused using a complete mathematical equations as shown in Table 1. For this work, we adopted Intel core I7-3770 working at 3.4 GHz and 12 GB RAM as a processor.

Moreover, using the proposed method in the case of electrically large-scaled structure and high frequency response, the SE

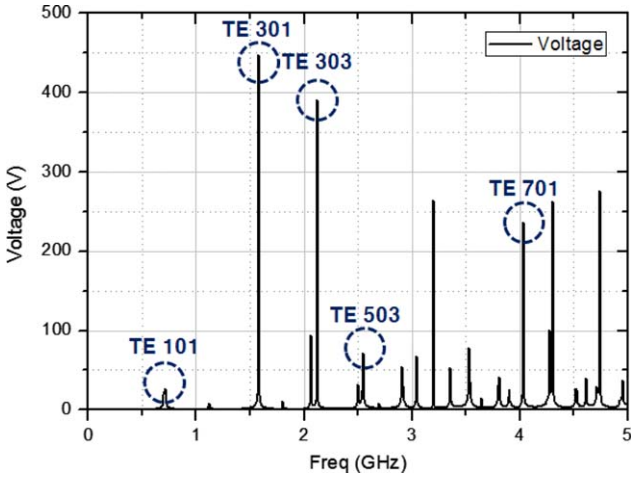

Figure 4 The resonant frequencies of single shielding cavity with an empty space. [Color figure can be viewed in the online issue, which is available at wileyonlinelibrary.com]

TABLE 1 Comparison of Time Consumption, Computational Resource, and Accuracy

Analysis Type	Time (s)	Memory (kB)	Accuracy
PWB method + BLT Eq (P&B)	0.76	47	Low
TL theory + BLT Eq (T&B)	110	104	High
Full-wave simulation (FDTD)	413	8,486,040	Ref.

estimation can be easily and fast performed and very helpful for fast prediction of SE level.

4. CONCLUSION

This letter presented a simple estimation method to predict the induced voltages on both sides of single TL inside shielding cavity. This simple estimation method, which is combining the statistically-based approaches and BLT equations, was proposed by considering the dependence of incidence and polarization angles. By performing the comparison of the data obtained from the equivalent TL model and commercially available software based on FDTD, a reasonably good agreement has been obtained in the view point of an averaged value. Moreover, using the proposed method in the case of electrically large-scaled structure and high frequency response, the SE estimation can be easily performed and very helpful for fast prediction of SE level.

REFERENCES

1. E. Liu, P.-A. Du, W. Liu, and D. Ren, Accuracy analysis of shielding effectiveness of enclosures with apertures: A parametric study, IEEE Trans Electromagn Compat 56 (2014) 1396–1403.
2. M.P. Robinson, T.M. Benson, C. Christopoulos, M.D. Ganley, A.C. Marvin, S.J. Porter, and D.W.P. Thomas, Analytical formulation for the shielding effectiveness of enclosures with apertures, IEEE Trans Electromagn Compat 40 (1998), 240–248.
3. D. Hill, Electromagnetic fields in cavities: Deterministic and statistical theories, IEEE Press, New York, NY, 2009.
4. D. Hill, Plane wave integral representation for fields in reverberation chambers, IEEE Trans Electromagn Compat 40 (1998), 209–217.
5. D. Pozar, Microwave engineering, Wiley, New York, 2005.
6. C. Hao and D. Li, Simplified model of shielding effectiveness of a cavity with apertures on different sides, IEEE Trans Electromagn Compat 56 (2014), 335–342.
7. R.N. Simons, Coplanar waveguide circuits, components, and systems, Wiley, New York, NY, 2001.
8. F.M. Tesche and C.M. Butler, On the addition of EM field propagation and coupling effects in the BLT equation, College of Engineering and Science, Note 588, 2003.
9. I. Junqua, J.P. Parmantier, and F. Issac, A network formulation of the power balance method for high-frequency coupling, Electromagnetics 25 (2007), 603–622.

HIGH EFFICIENCY POWER AMPLIFIER WITH FREQUENCY BAND SELECTIVE MATCHING NETWORKS

Junhyung Jeong, Phirun Kim, and Yongchae Jeong
Division of Electronics and Information Engineering, IT Convergence Research Center, Chonbuk National University, Jeonju, Republic of Korea; Corresponding author: ycjeong@jbnu.ac.kr

Received 2 February 2015

ABSTRACT: *In this article, a high efficiency power amplifier (PA) with frequency selective matching networks (MNs) that can provide*

passband impedance matching as well as suppression of out-of-band signals simultaneously is proposed. The proposed frequency selective MN consists of a λ/4 length coupled line, a λ/2 length open step-impedance resonator stub, and a λ/6 length bias line terminated with a bypass capacitor. For experimental validation, the PA with input and output frequency selective MNs is designed and fabricated for the US PCS band (1.93–1.99 GHz). The measurement results show that the output power and power add efficiency are 43 dBm and 70.3%, respectively, at the center frequency of 1.96 GHz, and the out-of-band suppression is higher than 32 dB. © 2015 Wiley Periodicals, Inc. Microwave Opt Technol Lett 57:2031–2034, 2015; View this article online at wileyonlinelibrary.com. DOI 10.1002/mop.29263

Key words: *coupled line; transmission zeros; wideband impedance transformer*

1. INTRODUCTION

As the frequency spectrum is limited for wireless systems, maximum and efficient utilization of the frequency spectrum assigned to communication service providers must be ensured. As modern wireless systems must transmit signals only on the permitted frequency bands, high power amplifiers (PA) are followed by a band pass filter (BPF) to minimize the interference or noise with adjacent bands and out-of-bands on communication standards. Generally, the cavity BPF has a low insertion loss caused by high quality (Q) factor. Whereas the band selection and out-of-bands suppression characteristics of the BPF can be improved by increasing a number of filter stage, the passband insertion loss is also increased. As a result, the insertion loss increment of the BPF deteriorates the overall system efficiency.

Conventionally, the PA and filter are independently designed based on a 50-Ω system impedance. Recently, the codesign approach of the PA and filter together was reported in [1]. The designed cavity BPF could provide the output impedance matching and band selection characteristics. However, it requires very high Q factor filters to ensure low insertion loss and complex structure due to output impedance of PA which is different with 50 Ω.

High efficiency PAs usually contain harmonic termination networks and input/output matching networks (MNs) [2–8]. Figure 1 shows the general RF PA block diagram. At the drain port of transistor, harmonics control network is designed by drain output voltage and current waves forming and then connected to the PA first for the high efficiency performance. Next, the output passband MN is connected.

An impedance transformer with wide out-of-band suppression is realized in [9]. However, this circuit can provide only a real-to-real impedance transformation and has the second spurious at the third harmonic frequency band. There are some limitations to using the high efficiency PA design directly. In the [10], the couple-line impedance transformer used at the output network of PA for the impedance matching and DC-block. But, it also did not consider harmonics termination that is essential for the high efficiency PA design.

If the PA can be designed with frequency selective MNs which can provide passband impedance matching, harmonics termination, and suppression of out-of-band signals, these frequency selective MNs can reduce the number of stage of cavity BPF at the RF transmitter and it can improve overall system efficiency. In this article, a novel design of the PA with frequency selective MNs is presented. The proposed frequency MN can provide passband impedance matching, frequency selection, and harmonics termination characteristics simultaneously with a single circuit. The theoretical analysis of the proposed frequency selective MN and experimental results of the PA with the frequency selective MNs are provided.

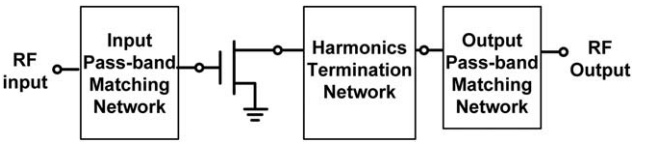

Figure 1 General RF PA block diagram

2. DESIGN EQUATION

Figure 2 shows the structures of the proposed PA and the frequency selective MN. The frequency selective MN consists of a $\lambda/4$ parallel coupled line, a $\lambda/2$ open step-impedance resonator (SIR) stub with impedances of Z_1 and Z_2, and a $\lambda/6$ bias line terminated with a bypass capacitor connected at input port 1. The reflection coefficient (S_{11}) and transmission coefficient (S_{21}) of the proposed network at the center frequency (f_0) can be expressed by (1) and (2), where Z_S indicates the source or load impedances ($Z_S \neq 50\ \Omega$) of the transistor obtained from the source- or load-pull methods, and Z_L is a termination port impedance ($Z_L = 50\ \Omega$).

$$S_{11}|_{f=f_0} = \frac{(Z_{0e}-Z_{0o})^2 - 4Z_S Z_L}{(Z_{0e}-Z_{0o})^2 + 4Z_S Z_L} \tag{1}$$

$$S_{21}|_{f=f_0} = \frac{-j4(Z_{0e}-Z_{0o})\sqrt{Z_L Z_S}}{4Z_S Z_L + (Z_{0e}-Z_{0o})^2} \tag{2}$$

where Z_{0e} and Z_{0o} are even- and odd-mode impedances of the coupled line, respectively.

The input impedance of MN at f_0 can be found as in (3).

$$Z_{in}|_{f=f_0} = \frac{(Z_{0e}-Z_{0o})^2}{4Z_L} \tag{3}$$

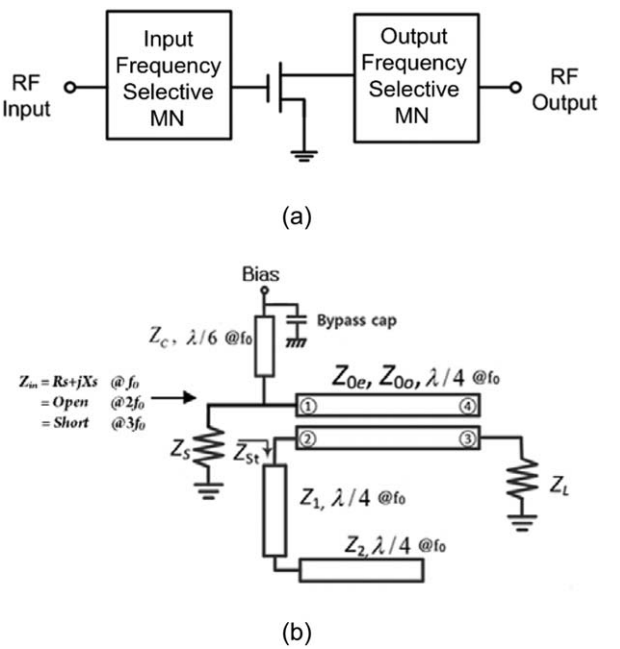

Figure 2 Proposed block diagrams of (a) PA and (b) frequency selective MN

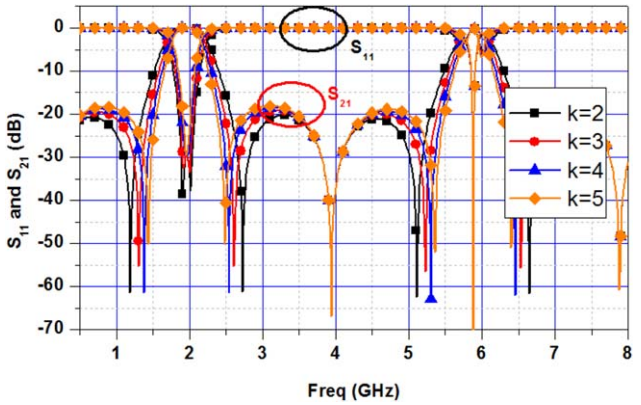

Figure 3 Simulated *S*-parameters of frequency selective output MN according to k (@$Z_S = 7.8-j2.5\ \Omega$, $Z_{0e} = 75.5\ \Omega$, $Z_{0o} = 35\ \Omega$, $Z_L = 50\ \Omega$, $Z_1 = 25\ \Omega$, and $Z_2 = [50, 75, 100, \text{and } 125\ \Omega]$). [Color figure can be viewed in the online issue, which is available at wileyonlinelibrary.com]

where Z_{0e} can be found as in (4) for the specific reflection coefficient (S_{11}), Z_{0o}, Z_L, and Z_S.

$$Z_{0e} = 2\sqrt{\frac{Z_S Z_L\left(1+S_{11}|_{f=f_0}\right)}{\left(1-S_{11}|_{f=f_0}\right)}} + Z_{0o} \tag{4}$$

Similarly, the transmission zeros of the proposed MN can be determined as in (5).

$$f_{TZ\_SIR} = \frac{2}{\pi}\cdot f_0\left(\sin^{-1}\sqrt{\frac{k}{1+k}} + n\pi\right) \quad (@n=0, 1, 2\cdots) \tag{5a}$$

$$f_{TZ\_CL} = (2+n)f_0 \quad (@n=0,\ 1, 2\cdots) \tag{5b}$$

where k, f_{TZ_SIR}, and f_{TZ_CL} are the impedance ratio of the SIR stub (Z_2/Z_1) and the transmission zero frequencies generated by the SIR stub and the coupled line, respectively. There are three

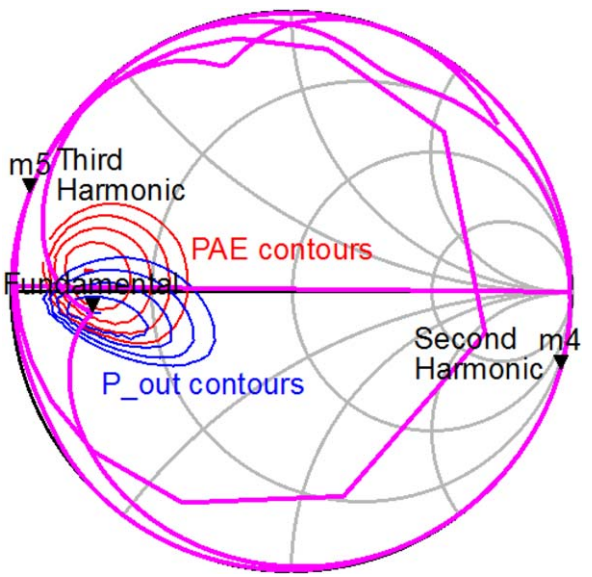

Figure 4 Simulated reflection coefficient of frequency selective MN ($k = 3$) and load-pull output power/PAE contours. [Color figure can be viewed in the online issue, which is available at wileyonlinelibrary.com]

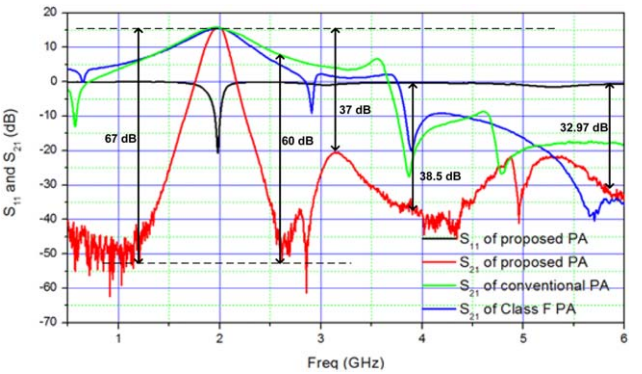

Figure 5 Comparison of measured small-signal frequency responses between the conventional, class F, and proposed PA. [Color figure can be viewed in the online issue, which is available at wileyonlinelibrary.com]

steps to match the optimum impedance ($Z_s = R_s + jX_s$) of the PA using the proposed frequency selective MN, which is described as follows.

a. Calculate Z_{0e} impedance using (4) with the specific wanted S_{11} by designer, the real part of the input impedance (R_S), and Z_{0o}.
b. Locate the transmission zeros near the passband by changing $k = Z_2/Z_1$ of the SIR stub.
c. Finally, match the imaginary part of the optimum impedances (X_s) by optimization of the k and bias line length.

3. SIMULATION AND MEASUREMENT RESULTS

For experimental validation, the proposed PA was designed with a 25-W GaN HEMT transistor (NPTB00025B) from Nitronex for the US PCS downlink band (1.93–1.99 GHz). The desired source impedance $Z_{inopt} = 3.5-j4.8$ and load impedance $Z_{outopt} = 7.8-j2.5$ at $f_0 = 1.96$ GHz were extracted from the source- and load-pull methods using ADS 2013. The circuit was fabricated on a RT/Duriod 5880 substrate from Rogers, with a dielectric constant (ε_r) of 2.2 and a thickness (h) of 31 mils.

Figure 3 shows the simulated frequency response of the frequency selective output MN according to k. As seen in the figure, the return loss at $f_0 = 1.96$ GHz is better than 30 dB. Similarly, the out-of-band signals are suppressed by transmission zeros located at 1.3, 2.6, 3.92, 5.25, and 5.88 GHz. As k increases, the out-of-band attenuation characteristic near the passband becomes steeper.

Figure 4 shows the simulated reflection coefficient (S_{11}) of the frequency selective output MN and the output power/power added efficiency (PAE) contours in the case of $k = 3$. As seen in the figure, the proposed MN is matched with the maximum power delivery impedance (Z_{outopt}). Moreover, the impedances at $2f_0$ and $3f_0$ are almost open-circuited and short-circuited, respectively, which can provide high efficiency characteristics in the PA design.

Figure 5 shows a comparison of the measured small-signal gain responses of the fabricated conventional PA, passband matched class F PA [11], and proposed PAs. The return loss of the proposed PA is higher than 21.92 dB at $f_0 = 1.96$ GHz. The frequency selective gain characteristics are achieved with a small-signal gain of 15.46 dB at f_0. Moreover, the signal attenuations at $2f_0$ and $3f_0$ are 38.5 dB and 32.97 dB, respectively, and the out-of-band signal suppression is more than 20 dB. The

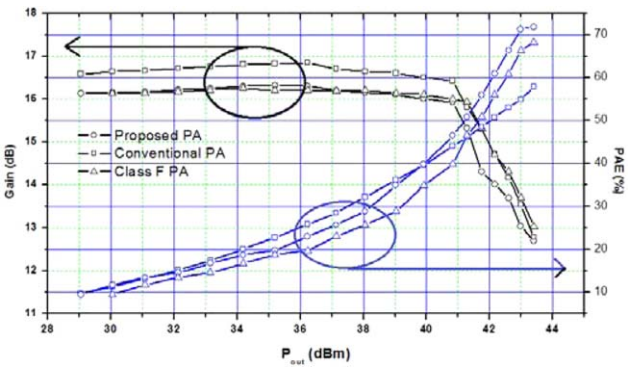

Figure 6 Measured power gain and PAE of conventional, class F, and proposed PA at 1.96 GHz. [Color figure can be viewed in the online issue, which is available at wileyonlinelibrary.com]

difference between the passband and out-of-band gains is more than 37 dB. In addition, a maximum 60-dB difference between the passband and the out-of-band gains is obtained at the transmission zero frequency of 2.6 GHz.

Figure 6 shows the measured gains and PAE performances of three PAs at f_0 according to the output powers. The measurement results show that the output power and PAE of the proposed PA are determined to be 43.1 dBm and 70.3%, respectively, at the 3-dB gain compression point, while the output power and PAE achieved using the conventional PA are 43.1 dBm and 57%, respectively. Similarly, class F PA output MN was designed using [11] structure. The 3-dB gain compression point output power and PAE of class F PA is 42.9 dBm and 68%, respectively.

Figure 7 shows photographs of the proposed PAs. The proposed PA has a slightly larger size, but the size of the $\lambda/2$ open SIR stub can be minimized with a meander transmission line structure.

4. CONCLUSION

In this article, the design of a PA with frequency selective MNs is described. With the frequency selective characteristics of the proposed MNs, the proposed PA provides sharp passband selective characteristics with out-of-band suppression. The proposed PA can achieve high efficiency and high power performance due to the proper harmonics termination. The proposed PA can also reduce the burden of the RF transmitting BPF. In microwave active circuits operated at higher than 10 GHz, a $\lambda/4$ parallel coupled line is generally used instead of a DC-blocking capacitor. Because the proposed frequency selective MN can be used as a DC-blocking capacitor as well as a MN and harmonics termination, simultaneously, the proposed MN can be applicable in microwave circuit design.

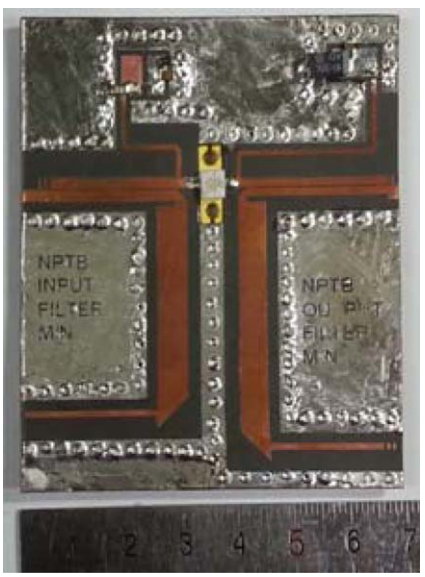

Figure 7 Photographs of proposed PA. [Color figure can be viewed in the online issue, which is available at wileyonlinelibrary.com]

REFERENCES

1. K. Chen, J. Lee, W.J. Chappell, and D. Peroulis, Co-design of highly efficiency power amplifier and high-Q output bandpass filter, IEEE Trans Microwave Theory Tech 61 (2013), 3940–3950.
2. V. Carrubba, J. Lees, J. Benedikt, P.J. Tasker, and S.C. Cripps, A novel highly efficient broadband continuous class-F RF PA delivering 74% average efficiency for an octave bandwidth, In: IEEE MTT-S International Microwave Symposium Digest, Baltimore, MD, 2011, pp. 1–4.
3. A.N. Rudiakova and V.G. Krizhanovski, Driving waveforms for class-F power amplifiers, In: IEEE MTT-S International Microwave Symposium Digest, Boston, MA, 2000, pp. 473–476.
4. H. Choi, S. Shim, Y. Jeong, J. Lim, and C.D. Kim, A compact DGS load-network for highly efficient class-E power amplifier, In: Proceedings of European Microwave Conference, Rome, 2009, pp. 492–495.
5. F.H. Raab, Class-E, class-C, and class-F power amplifiers based upon a finite number of harmonics, IEEE Trans Microwave Theory Tech 49 (2001), 1462–1468.
6. S.F. Ooi, S.K. Lee, A. Sambell, E. Korolkiewicz, and P. Butterworth, Design of a high efficiency power amplifier with input and output harmonic terminations, Microwave Opt Technol Lett 49 (2007), 391–395.
7. D. Schmelzer and S.I. Long, A GaN HEMT class-F amplifier at 2 GHz with $>80\%$ PAE, IEEE J Solid-State Circuits 42 (2007), 2130–2136.
8. A. Inoue, A. Ohta, S. Goto, T. Ishikawa, and Y. Matsuda, The efficiency of class-F and inverse class-F amplifiers, In: IEEE MTT-S International Microwave Symposium Digest, Fort Worth, TX, 2004, pp. 1947–1950.
9. P. Kim, G. Chaudhary, and Y. Jeong, Wideband impedance transformer with out-of-band suppression characteristics, Microwave Opt Technol Lett 56 (2014), 2612–2616.
10. Y. Wu, Y. Liu, S. Li, and S. Li, A novel high-power amplifier using a generalized coupled-line transformer with inherent DC-block function, Prog Electromagn Res 119 (2011), 171–190.
11. Y. Jeong, G. Chaudhary, and J. Lm, A dual band high efficiency class-F GaN power amplifier using a novel harmonic-rejection load network, IEICE Trans Electron E95-C (2012), 1783–1789.

DUAL-BAND WILKINSON POWER DIVIDER CONSTRUCTED USING I-SHAPED LINES

Kuo-Sheng Chin, Tzu-Chiang Lin, Chih-Chun Chang, Yu-Chung Wang, Hao-Che Kuo, and Jyun-Yi Hu
Department of Electronic Engineering, Chang Gung University, No. 259 Wen-Hwa 1st Road, Kwei-Shan, Taoyuan 333, Taiwan, Republic of China; Corresponding author: kschin@mail.cgu.edu.tw

Received 2 February 2015

ABSTRACT: *Dual-band Wilkinson power dividers were constructed using I-shaped lines. Inserting a stepped-impedance stub in the middle of the lines could induce a shunt susceptance to achieve dual-band 90°*